JOURNAL OF SOLID STATE CHEMISTRY 115, 353–359 (1995)

Preparation, Crystal Structure, and Properties of a New Double Metal Nitride, SrNiN, and of $Ca_{1-x}Sr_xNiN$ ($0 \leq x \leq 0.5$) Solid Solutions

T. Yamamoto,[1] S. Kikkawa,[2] and F. Kanamaru

Institute of Scientific and Industrial Research, Osaka University, Osaka 567, Japan

Received May 16, 1994; in revised form August 5, 1994; accepted August 11, 1994

A new double metal nitride, SrNiN, and solid solutions $Ca_{1-x}Sr_xNiN$ ($0 \leq x \leq 0.5$) were prepared by the reaction of Sr_2N and/or α-Ca_3N_2 with nickel fine powder in a nitrogen atmosphere. SrNiN had an orthorhombic crystal lattice, *Pnma*, with a = 9.0859 Å, and b = 13.231 Å, and c = 5.2473 Å and was isostructural with BaNiN. The present products have crystal structures composed of infinite $[NiN_{2/2}]^{2-}$ chains linked with tetrahedrally coordinated Sr^{2+} and/or Ca^{2+}. The chain shapes are zigzag in SrNiN and linear in $Ca_{1-x}Sr_xNiN$ ($0 \leq x \leq 0.5$). Both crystal lattices have fcc nitrogen packing. The difference in chain shape can be understood in terms of a limited range of distortion in the tetrahedron supporting $[NiN_{2/2}]^{2-}$ chains. All of these products were metallic conductors with residual electrical resistivities of order 10^{-4} Ω cm at 10 K. Electrical resistivities at room temperature were 6.0×10^{-3} Ω cm in SrNiN and $2–6 \times 10^{-4}$ Ω cm in $Ca_{1-x}Sr_xNiN$. They showed temperature-independent magnetic behavior at temperatures down to 77 K.

1. INTRODUCTION

The recently discovered compound CaNiN is a metallic conductor (1) in which one-dimensional Ni–N chains form layers stacking along the c-axis as shown in Fig. 1. However, its band structure is rather three-dimensional and Peierls instability was not observed at temperatures down to 4.2 K. LAPW calculation indicated that interchain coupling strongly reduced the tendency to instability related to low dimensionality (2). The crystal structure was related to that of anti-perovskite-type nitrides such as Ca_3BiN and a band calculation was performed to determine the possibility of a new high-T_c superconductor (3). The formal valence of the Ni cation is +1 in CaNiN. This is very uncommon in Ni oxides; its electron configuration is d^9, which is the same as that of Cu^{2+} in high-temperature superconductors. The presence of BaNiN had been very briefly reported (4). The compound was not isostructural with CaNiN and had zigzag Ni–N infinite chains. The structural relation between CaNiN and BaNiN has been very difficult to understand. We have briefly reported only the occurrence of $Ca_{1-x}Sr_xNiN$ solid solutions and a new compound SrNiN (5).

In the present paper, we will analyze the crystal structure of these alkaline-earth nickel nitride ANiN systems. The structural aspects and their bond natures will be discussed in relation to their electrical and magnetic properties.

2. EXPERIMENTAL

Calcium nitride, α-Ca_3N_2, and strontium nitride, Sr_2N, were prepared, respectively, by heating calcium metal (Showa Electric Ind. Ltd., 99.99%) and strontium metal granules (Nacalai Tesque Co. Ltd., 99.9%) under N_2 gas (Osaka Oxygen Ind. Ltd., 99.9999%). They were heated to 573 K under vacuum and reacted under N_2 for 2–3 hr, monitoring outlet N_2 flow rate in temperature ranges of 948–1223 K for Ca_3N_2 and 643–873 K for Sr_2N. All operations except the firing process were carried out in an argon-filled glove box. Red-brown α-Ca_3N_2 having an anti-rare-earth C-type cubic lattice with a = 11.47 Å and black Sr_2N having an anti-CdI_2-type hexagonal lattice with a = 3.58 Å and c = 20.69 Å were obtained. These lattice parameters agreed with the previously reported values (6, 7). Their nitrogen contents were estimated to be $Ca_3N_{1.98}$ and $Sr_2N_{1.0}$, respectively, using a modified Dumas method.

These alkaline-earth nitrides were mixed with submicrometer-size Ni metal powder (Aldrich Co. Ltd., 99.9%) in appropriate molar ratios. The starting mixtures were pressed into pellets and heated at 1273 K under N_2 gas for 20–36 hr. The pellets were sandwiched or covered with powder of the same composition to prevent oxidation and evaporation of the alkaline-earth metals in the pellets.

[1] Present address: Central Research Institute of Electric Power Industry, Yokosuka 240-01, Japan.

[2] To whom correspondence should be addressed.

0022-4596/95 $6.00

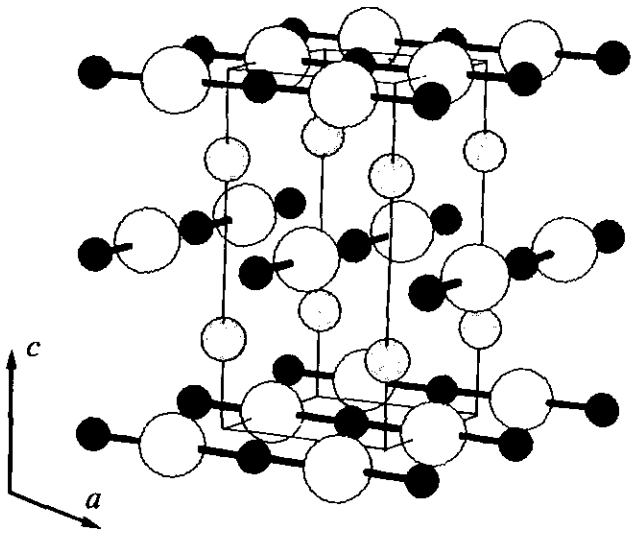

FIG. 1. Schematic representation of the crystal structure of CaNiN. Open, filled, and shaded circles represent nitrogen, nickel, and calcium atoms, respectively.

Strontium nitride is more easily oxidized than calcium nitride. To reduce the oxide contamination in SrNiN, the starting mixture was heated to 473 K under vacuum, reacted at 1273 K for 12–15 hr under N_2, and then cooled to room temperature for 1 hr.

The products were identified by a powder X-ray diffraction method using a diffractometer with Cu$K\alpha$ radiation monochromatized with pyrolytic graphite. Intensity data were collected in step-scan mode at room temperature. The sample loaded on a silica glass plate was set in a holder covered with a 0.007-mm-thick aluminum window to prevent air exposure. The lattice parameters were refined by Rietveld analysis using the computer program RIETAN. Least-squares refinement was performed using a pseudo-Voigt profile function adjusting the mixing parameter.

Electrical resistivity was measured on sintered pellets ($5 \times 15 \times 0.5$ mm) by the four-probe method in the temperature range from 10 to 300 K. A constant dc current of 0.1–10 mA was supplied through silver electrodes. The samples were loaded into an argon-filled metal holder, and the measurements were performed through the lead wire. The temperature was monitored with a Au–Fe–Chromel thermocouple. Temperature dependence of magnetic susceptibility was measured using a Faraday balance in the temperature range from 70 to 300 K in a field of 1–14 kOe. The powder sample was sealed in an evacuated silica glass capsule and then loaded into a holder. We corrected for diamagnetic contributions of the silica glass.

3. RESULTS AND DISCUSSIONS

3.1. Preparation, Crystal Structure, and Properties of SrNiN with a Zigzag $[NiN_{2/2}]^{2-}$ Chain

The product in the Sr_2N–Ni system was black and more stable in air than strontium nitride. Chemical analysis showed its nitrogen content to be $SrNiN_{1.0}$. Its PXD pattern could be indexed with an orthorhombic unit cell as shown in Table 1. The structure was analyzed in space group *Pnma* (No. 62) similarly to BaNiN using the Rietveld method. The refinement was done in two stages; the atomic coordinates and thermal parameters were refined in the first step, with other parameters kept fixed. After these parameters converge to their optimum values, parameters such as scale, background, half-width, and unit cell dimensions were refined. Temperature factors B for N1 and N2 sites were refined assuming they had the same value; otherwise the refinement was unstable. Finally, a total of 31 positional, thermal, and instrumental parameters were refined. Results for the refinement are summarized in Tables 2 and 3. The lattice parameters were a = 9.0859(4) Å, b = 13.230(93) Å, c = 5.2473(3) Å. The observed PXD agreed very well with the simulation, as shown in Fig. 2. Interatomic distances and bond angles are listed in Table 4.

The crystal structure of SrNiN is characterized by infinite $[NiN_{2/2}]^{2-}$ zigzag chains as depicted in Fig. 3. It is isostructural with that of BaNiN but fairly distorted. The $[NiN_{2/2}]^{2-}$ chains run along the [010] direction with an inclination angle of ±62° to the a-axis. The chains form zigzag planes stacked in parallel along the a-axis. Along the [100] direction the zigzag planes are piled up to form

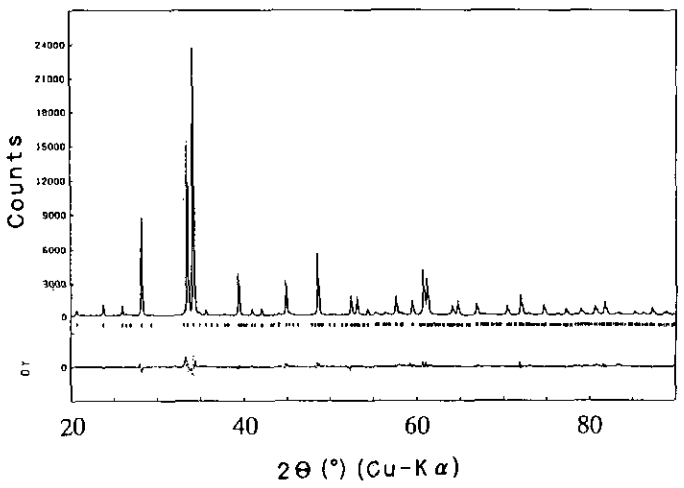

FIG. 2. Observed PXD with the difference between the observation and the calculation for SrNiN.

TABLE 1
X-Ray Powder Diffraction Data for SrNiN[a]

h	k	l	d_{calc}	d_{obs}	I/I_0	h	k	l	d_{calc}	d_{obs}	I/I_0	h	k	l	d_{calc}	d_{obs}	I/I_0
1	1	1	4.298	4.279	3	4	4	1	1.763	1.761	2	4	7	1	1.400		
1	2	1	3.746	3.732	5	2	7	0	1.745	1.742	8	2	9	0	1.399	1.397	4
2	0	1	3.435	3.424	5	1	7	1	1.745			1	9	1	1.399		
1	3	1	3.165	3.155	37	4	5	0	1.724	1.722	7	4	0	3	1.386	1.384	1
2	3	0	3.164			2	5	2	1.724			4	8	0	1.337	1.336	4
				2.978	3	3	6	1	1.688	1.686	3	2	8	2	1.337		
				2.751	3	0	6	2	1.688			6	0	2	1.312	1.311	7
2	4	0	2.674	2.668	63	0	3	3	1.627	1.623	1	0	0	4	1.312		
1	4	1	2.674			5	3	1	1.600			5	7	1	1.271	1.270	4
0	0	2	2.624	2.618	100	4	3	2	1.600	1.598	6	4	7	2	1.271		
3	0	1	2.623			1	3	3	1.600			3	6	3	1.249	1.247	2
3	1	1	2.573	2.567	4	2	8	0	1.554	1.552	6	6	6	0	1.248		
				2.516	3	1	8	1	1.554			4	9	0	1.234	1.234	3
2	5	0	2.287	2.282	16	5	4	1	1.524			2	9	2	1.234		
1	5	1	2.287			4	4	2	1.524	1.522	16	7	3	1	1.212		
0	6	0	2.201	2.201	2	1	4	3	1.524			5	3	3	1.212	1.211	3
4	2	0	2.149	2.143	3	3	0	3	1.515	1.513	13	2	3	4	1.212		
2	2	2	2.149			6	0	0	1.514								
0	6	1	2.033	2.032	6	4	7	0	1.453	1.451	4						
4	3	0	2.019	2.016	13	4	5	2	1.441								
4	4	0	1.872	1.870	23	1	5	3	1.441	1.440	5						
1	5	2	1.825	1.821	2	5	5	1	1.440								

[a] *Pnma*: a = 9.0859(4) Å, b = 13.230(93) Å, and c = 5.2473(3) Å.

columns, changing the sign of their inclination to the a-axis. Sr atoms are coordinated by four nitrogen atoms in the neighboring zigzag $[NiN_{2/2}]^{2-}$ chains. Two kinds of Ni atoms form the $[NiN_{2/2}]^{2-}$ chains. Ni1 is coordinated with two kinds of nitrogen atoms, N1 and N2. Interatomic distances Ni1–N1 and Ni1–N2 along a chain were 1.83 and 1.89 Å, as shown in Table 4. The coordination around Ni1 was not exactly linear. However, Ni2 is linearly surrounded by two N1 atoms having a distance of 1.77 Å. The Ni–N distance is longer around the zigzag corner than in the straight chain section. The distances are shorter than those expected from the ionic or atomic radii of Ni and N. The bonds between the Ni and N atoms are strongly covalent. The bond angles were 180°, 177°, and 78° for N1–Ni2–N1, N1–Ni1–N2, and the corner Ni1–N2–Ni1. π-interaction may be important for the linear bond around Ni atoms, but the bending at the corner is unfavorable to π-interaction between Ni1 and N atoms,

TABLE 2
Rietveld Analysis Results for SrNiN

Scale factor		0.000363(2)
FWHM parameter	U	0.078(9)
(Half-width parameter)	V	0.046(3)
	W	0.0272(9)
Asymmetry parameter	A	0.03(5)
Gaussian fraction	γ	0.42(2)
FWHM (Gauss)/FWHM (Lorentz)	δ	1.38(5)
Lattice constants	a(Å)	9.0859(4)
	b(Å)	13.230(93)
	c(Å)	5.2473(3)
Cell volume	V(Å^3)	630.802(4)
Weighted pattern R-factor	R_{WP}	12.58
Pattern R-factor	R_P	8.96
Expected R-factor	R_E	3.59
Integrated intensity R-factor	R_I	1.94
Structural factor R-factor	R_F	3.27

TABLE 3
Fractional Coordinates after Rietveld Analysis

Atom	Site	Occupancy	Fractional coordinates x	y	z	B(Å^2)
Sr(1)	8*d*	1.0	0.336(2)	0.0874(3)	0.978(1)	0.02(8)
Sr(2)	4*c*	1.0	0.512(1)	0.25	0.500(2)	0.02(8)
Ni(1)	8*d*	1.0	0.170(2)	0.1602(2)	0.467(2)	0.02(8)
Ni(2)	4*a*	1.0	0	0	0	0.02(8)
N(1)	8*d*	1.0	0.101(6)	0.075(3)	0.217(9)	0.02(8)
N(2)	4*c*	1.0	2.30(7)	0.25	0.73(1)	0.02(8)

TABLE 4
Calculated Bond Distances (Å) and Angles (°) for SrNiN

Environment around Sr(1) (8*d*)					
Sr1–N1	× 1	2.49(6)	N1–Sr1–N1	× 1	93.5(15)
	× 1	2.61(5)		× 1	113.6(17)
	× 1	2.89(6)		× 1	115.7(15)
Sr1–N2	× 1	2.70(5)	N1–Sr1–N2	× 1	89.6(17)
N1–N1	× 1	4.01(7)		× 1	127.7(16)
	× 1	4.27(7)			
	× 1	4.56(8)			
N1–N2	× 1	3.66(7)			
	× 1	4.57(4)			
	× 1	5.02(8)			
Environment around Sr(2) (4*c*)					
Sr2–N1	× 2	2.70(4)	N1–Sr2–N1	× 1	117.8(15)
Sr2–N2	× 1	2.45(6)	N1–Sr2–N2	× 1	90.4(14)
	× 1	2.82(6)		× 2	116.6(14)
N1–N1	× 1	4.63(5)	N2–Sr2–N2	× 1	119.1(21)
N2–N2	× 1	4.55(9)			
N1–N2	× 2	3.66(7)			
	× 2	4.70(7)			
Environment around Ni(1) (8*d*)					
Ni1–N1	× 1	1.83(4)	N1–Ni1–N2	× 1	177.0(27)
Ni1–N2	× 1	1.89(5)			
Environment around Ni(2) (4*a*)					
Ni2–N1	× 2	1.77(4)	N1–Ni2–N1	× 1	180.0(20)
Environment around N(1) (8*d*)					
N1–Sr1	× 1	2.61(5)	Ni1–N1–Ni2	× 1	168.6(35)
	× 1	2.49(5)	Sr1–N1–Sr1	× 1	97.4(17)
	× 1	2.89(6)	Sr1–N1–Sr2	× 1	172.4(21)
N1–Sr2	× 1	2.70(4)		× 1	89.3(14)
N1–Ni1	× 1	1.83(4)		× 1	86.4(14)
N1–Ni2	× 1	1.77(4)	Sr1–N1–Ni1	× 1	93.2(19)
			Sr1–N1–Ni2	× 1	89.4(14)
Environment around N(2) (4*c*)					
N2–Sr1	× 2	2.70(4)	Ni1–N2–Ni1	× 1	78.1(26)
N2–Sr2	× 1	2.45(6)	Sr1–N2–Sr1	× 1	105.4(22)
	× 1	2.82(6)	Sr2–N2–Sr2	× 1	168.8(29)
N2–Ni1	× 2	1.89(5)	Sr1–N2–Ni1	× 2	87.5(4)
Ni1–Ni1	× 1	2.37(1)	Sr2–N2–Ni2	× 2	100.8(23)

resulting in electron localization around Ni1 atoms. A remarkably short distance of 2.37 Å was present between the Ni1 atoms coordinating to the common N2 in the *cis* position. It is shorter than 2.41 Å in BaNiN and comparable to the distance of Ni-metal direct bonding (2.308 Å).

There are two kinds of Sr atoms in SrNiN. Sr1 is coordinated by three N1 and one N2, and Sr2 is coordinated by two N1 and two N2. The interatomic distances between Sr and N atoms were in the range 2.45–2.89 Å. Ba atoms are located almost at the center of the parallel $[NiN_{2/2}]^{2-}$ zigzag planes in BaNiN, but the Sr atoms are well off from the center plane in SrNiN. The Sr atoms were slightly shifted to either the upper or the lower $[NiN_{2/2}]^{2-}$ zigzag plane. The corner N2 has the shortest bond distance to Sr2 among the Sr–N distances and the longest distance to Ni1 among the Ni–N distances. The displacement of the Sr atom may stabilize the corner N2 atom with the above-mentioned Ni1 interactions. Nitrogen atoms are sixfold coordinated in (NSr_4Ni_2) octahedra. The nickel atoms are in *cis* and *trans* positions around N2 and N1, respectively. Bond angles around nitrogen atoms have almost the ideal octahedral values with deviations of less than ±10°.

Electrical resistivity σ was measured in the temperature range from 10 to 300 K. At room temperature $\sigma = 6.0 \times 10^{-3}$ Ω cm, and it sharply decreased with decreasing temperature, as shown in Fig. 4. The temperature dependence was proportional to T^n ($n > 1$). There was a residual resistivity of 5.5×10^{-4} Ω cm at 10 K. Magnetic susceptibility was measured in the temperature range down to 77 K. The contribution of ferromagnetic impurity was subtracted from the data by the von Bernus (8) method, assuming 0.06 wt% of unreacted nickel. Temperature-independent weak paramagnetism of 6.8×10^{-6} emu/g resulted after the impurity correction. The magnetism is due to the conduction electrons observed for metallic conduction in SrNiN.

3.2. *Formation of $Ca_{1-x}Sr_xNiN$ Solid Solution with $[NiN_{2/2}]^{2-}$ Straight Chain*

The solid solution $Ca_{1-x}Sr_xNiN$ with a CaNiN-type tetragonal lattice was obtained in a limited compositional

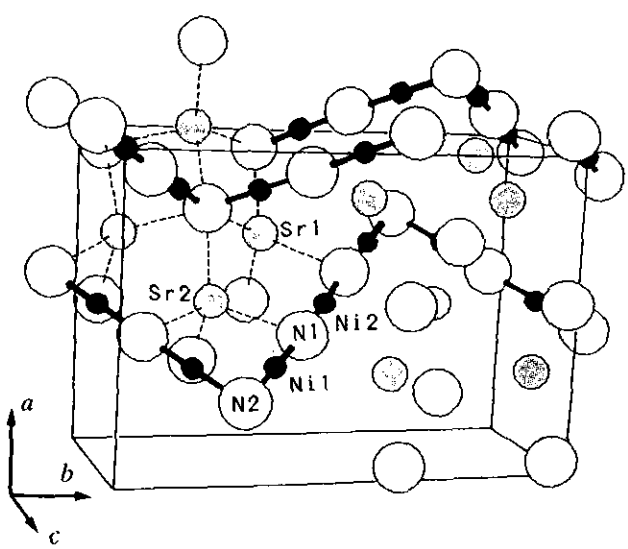

FIG. 3. Schematic crystal structure of SrNiN. Open, filled, and shaded circles represent nitrogen, nickel, and strontium atoms, respectively.

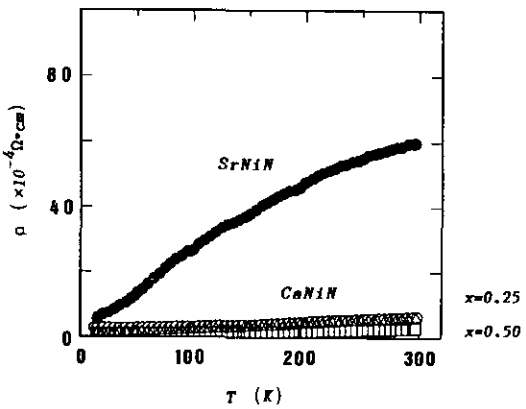

FIG. 4. Temperature dependences of electrical resistivity for SrNiN, CaNiN, and the solid solutions $Ca_{1-x}Sr_xNiN$. Filled circles, open circles, triangles, and squares represent the values for SrNiN, CaNiN, and the solid solutions with $x = 0.25$ and $x = 0.50$, respectively.

range up to $x = 0.50$. The products were contaminated by a small amount of CaO and SrO and a trace amount of Ni metal. The lattice constants $a = 3.5807(2)$ Å and $c = 7.0079(7)$ Å at $x = 0$ were the same, with the reported values $a = 3.5809(2)$ Å and $c = 7.0096(3)$ Å for CaNiN (1). The lattice constant c increased remarkably but the a constant also increased slightly with increased of strontium content x, as shown in Fig. 5. The lattice constants were $a = 3.6063$ Å and $c = 7.3415$ Å at $x = 0.5$. The solid solution limit was estimated to be $x = 0.50$. The value had been assumed to be $x = 0.75$ in our previous paper due to a small amount of calcium impurity (5). The c/a ratio also increased with x from 1.957 at $x = 0$ to 2.036 at $x = 0.5$. The $[NiN_{2/2}]^{2-}$ layers are formed with the $[NiN_{2/2}]^{2-}$ chains running along ⟨100⟩ and ⟨010⟩. The interlayer distance can easily expand but the a-axis, corresponding to twice the Ni–N distance in a chain, expands very slightly with the replacement of Ca^{2+} with Sr^{2+}.

The Ni–N distances in a chain ranged from 1.7904 to 1.8032 Å and were much shorter than $d_{Ni-N} = 1.83$ Å in Ni_2N, where Ni–N linear chains are also present in bct Ni lattice (9). These values were shorter than the sum of the single-bond Ni metallic radius (1.154 Å) and the covalent radius of N (0.70 Å) (10). The p orbitals of nitrogen may have π-interaction with d orbitals of nickel as well as σ-interaction (7). The straight $[NiN_{2/2}]^{2-}$ chains run parallel to each other in a $[NiN_{2/2}]^{2-}$ layer in the CaNiN-type structure, as shown in Fig. 1. They are perpendicular to each other through alkaline-earth atoms. The alkaline-earth atoms were tetrahedrally coordinated with four N atoms. The N–N distance between the neighboring $[NiN_{2/2}]^{2-}$ chains in a layer is shorter than the interlayer N–N distance. The N_4 tetrahedron is elongated along the c-axis. The deviation from an ideal tetrahedron increases with increasing Sr content because the Ca(Sr)–N distance can expand but the Ni–N distance is not elongated as much. The A–N (A = Ca, Sr) distances ranged from 2.50 to 2.57 Å. They were comparable to an expected value of 2.46 Å for the ionic radius sum of Ca^{2+} and N^{3-} (11). Calcium atoms are partially ionized, supplying their electrons to Ni–N covalent bonds through nitrogen atoms.

CaNiN and all solid solutions $Ca_{1-x}Sr_xNiN$ showed metallic behavior down to 10 K, as shown in Fig. 4. The magnitude of the electrical resistivity slightly decreased with increasing strontium content x. It was on the order of 10^{-4} Ω cm up to $x = 0.5$ at room temperature. Similar behavior has been reported for CaNiN (1). The residual resistivity ratio $\sigma_{300\,K}/\sigma_{10\,K}$ was around 3. The ratio was half the reported value in the present product. The residual resistivities were in the range $1–3 \times 10^{-4}$ Ω cm at 10 K and were of the same order as that of SrNiN having the zigzag $[NiN_{2/2}]^{2-}$ chain.

Temperature-independent magnetism was observed on both CaNiN and $Ca_{0.5}Sr_{0.5}NiN$ after correction for the ferromagnetic contribution. The presence of the ferromagnetic impurity in CaNiN was reported by Chern and Disalvo (1), who found a temperature-dependent paramagnetic contribution even after the impurity correction. The reported magnetic moment of 0.39 μ_B is too small to be explained by the intrinsic moment of Ni^+. Susceptibility for the present CaNiN was 26.5×10^{-6} emu/g at temperatures between 77 and 300 K. This is half the reported value, but of the same order of magnitude. Pauli paramagnetism is reasonable because CaNiN is a metallic conductor. The susceptibility value seems to be too large for the Pauli-paramagnetic contribution, probably because the ferromagnetic contribution could not be fully removed. $Ca_{0.5}Sr_{0.5}NiN$ was also Pauli-paramagnetic and

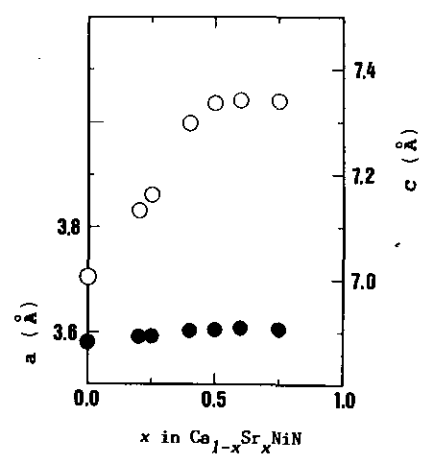

FIG. 5. Tetragonal lattice constants a and c plotted against the amount of strontium x in $Ca_{1-x}Sr_xNiN$ solid solution. Filled and open circles represent a and c parameters, respectively.

its susceptibility was 1.22×10^{-6} emu/g. The magnitude of the Pauli-paramagnetic susceptibility can generally be related to the conduction electron density at a Fermi surface. There are small differences in the susceptibility between CaNiN, $Ca_{0.5}Sr_{0.5}NiN$,and SrNiN. However, the presence of a ferromagnetic impurity makes discussion of conduction electron density difficult.

3.3. Structural Relation of SrNiN to CaNiN

Most metal nitrides containing alkali and alkaline-earth metals have a fcc nitrogen matrix. α-Ca_3N_2 has an anti-rare-earth C-type structure which can be related to the anti-fluorite structure. Calcium atoms occupy two-thirds of the tetragonal holes in the fcc nitrogen packing. CaNiN has a structure related to α-Ca_3N_2. Calcium atoms occupy half of the tetrahedral holes. The nickel atoms are displaced from the centers to the edges of the tetrahedra in a cubic close-packed nitrogen matrix to be linearly coordinated by two nitrogen atoms.

The crystal structure of SrNiN is intimately related to that of CaNiN, containing infinite linear $[NiN_{2/2}]^{2-}$ chains. Nitrogen atoms in SrNiN also form a distorted fcc lattice and strontium atoms occupy half of its tetrahedral holes. Nickel atoms shift their position from the center to the edge in the tetrahedra as in the case of CaNiN. CaNiN and SrNiN have different chain shapes; they are infinite straight and zigzag, respectively. Nitrogen atoms construct a distorted face-centered cubic arrangement in which the calcium or the strontium atoms occupy half of the tetrahedral holes. The nickel atoms are on the edges of the other half of the tetrahedra forming $[NiN_{2/2}]^{2-}$. The $[NiN_{2/2}]^{2-}$ chains run parallel to each other in the (001) plane of the CaNiN and the (110) plane of SrNiN. The planar arrays of the chains are stacked in the *a*-direction in SrNiN as mentioned above but along the *c*-direction in CaNiN. These $[NiN_{2/2}]^{2-}$ planes are separated from each other by square arrays of Ca or Sr atoms. The largest difference in the structures is the chain shape between CaNiN and SrNiN. However, the zigzag Ni–N chains in SrNiN can be related to the linear chains of CaNiN by folding in every six Ni–N units at the (101) plane of the fcc nitrogen matrix. Sr atoms also became equivalent through the folding operation and then the whole lattice has to be slightly distorted. The zigzag $[NiN_{2/2}]^{2-}$ chain distorts the SrN_4 tetrahedron in SrNiN. The Ni–Ni distances were 3.58 Å in a chain and 3.50 Å across the chains in CaNiN. They correspond to the N–N distances. The N_4 tetrahedron is elongated along the *c*-axis with increased *x* in $Ca_{1-x}Sr_xNiN$ up to $x = 0.5$, where the distances are 3.60, and 3.67 Å, respectively.

The Ni–Ni distances are 3.63 Å in a Ni–N chain and 3.67 Å across the chains in SrNiN. The former value agrees with the expected value of 3.63 Å for the hypothetical SrNiN with CaNiN-type structure estimated from the extrapolation of the data in Fig. 5. The latter value is remarkably smaller than the expected value of 3.83 Å of the $Ca_{0.5}Sr_{0.5}NiN$ in solid solution. It corresponds to the value for the $Ca_{0.5}Sr_{0.5}NiN$ solid solution, 3.6 Å. The ratio of N–N distances in a $[NiN_{2/2}]^{2-}$ chain $d_{N-N(c)}$ and the values between the $[NiN_{2/2}]^{2-}$ layers $d_{N-N(l)}$ are plotted against *x* as shown in Fig. 6. The value is 1.20 and the CaN_4 tetrahedron is elongated along the layer-stacking direction in CaNiN. The ratio increases to 1.23 at $x = 0.5$ with substitution of Sr^{2+} for Ca^{2+}. There are distributions of N–N distances in both SrNiN and BaNiN. Their average values are 1.21 and 1.20, respectively. The values in $Ca_{1-x}Sr_xNiN$ do not exceed the average values. The AN_4 tetrahedron seems not to be allowed to distort more than a certain limit. The distance $d_{N-N(c)}$ is twice that of the Ni–N bond distance in a linear chain in a CaNiN-type structure. It does not change much because of the covalent nature of the Ni–N bond. The distance $d_{N-N(l)}$ can expand to a certain limit with the substitution of alkaline-earth ion. The linear $[NiN_{2/2}]^{2-}$ chain may have to be folded to keep the tetrahedral environment around alkaline-earth ions.

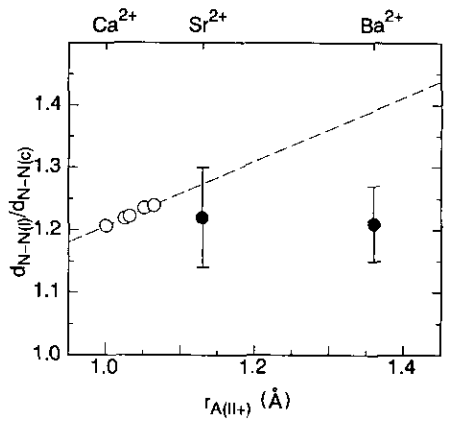

FIG. 6. Distortions of the AN_4 tetrahedron in various kinds of ANiN-type compounds. The vertical axis represents the ratio of N–N distances in a $[NiN_{2/2}]^{2-}$ chain and between the $[NiN_{2/2}]^{2-}$ layers. There are ranges of values in SrNiN and BaNiN because of the zigzag Ni–N chains. Filled circles represent their averages.

4. CONCLUSION

A new double metal nitride, SrNiN, was prepared by combining Ni metal and Sr_2N. It has an orthorhombic cell (*Pnma*, No. 62), with $a = 9.0859(4)$ Å, $b = 13.230(93)$ Å, and $c = 5.2473(3)$ Å and fcc nitrogen packing similar to that of α-Ca_3N_2 and CaNiN. The crystal structure was characterized by infinite $[NiN_{2/2}]^{2-}$ zigzag chains and in-

terchain Sr atoms coordinated by four nitrogens in the $[NiN_{2/2}]^{2-}$ chains. Comparison of the interatomic distances in SrNiN with those in $Ca_{1-x}Sr_xNiN$ solid solution products showed that the zigzag shape may result from size matching between the chain and the tetrahedron. The compound SrNiN was a metallic conductor with Pauli-paramagnetic behavior.

Two nitrogen atoms are linearly coordinated to nickel atoms in all *A*NiN. They form a σ-bond using the $2p_z$ orbital of nitrogen through hybridization of the $3d_{z2}$ and $4s$ orbitals of nickel. The valence of nickel is formally Ni^+ with $3d^9$. An unpaired electron is accommodated in an anti-bonding σ^* or π^* orbital to make the compound metallic. The *d*-character of calcium contributes to the lowest free-electron-like band at the Γ point, as pointed out in the previous electronic structure calculation for CaNiN (2). Interchain coupling also occurs through N–N interaction, either directly in the case of interactions within a layer or through the Ca ion in the case of interlayer coupling. Direct bonding may also be present between Ni1 atoms coordinating to the common N2 in SrNiN. Alkaline-earth metals are tetrahedrally coordinated by four nitrogen atoms with the bond distance *A*–N in the range 2.50–2.57 Å in CaNiN and the range 2.45–2.89 Å in SrNiN. These values are comparable to the radius sum 2.46 Å for Ca–N and 2.64 Å for Sr–N (11). The zigzag chain in SrNiN may be formed to preserve both the linear coordination around nickel and the tetrahedral coordination around strontium.

ACKNOWLEDGMENTS

We express our thanks to Mr. Imabayashi at Showa Electric Ind. Ltd. for supplying calcium granules of high purity. The authors also thank Professors O. Yamamoto and Y. Takeda at Mie University for magnetic measurements and Mrs. F. Fukuda at MAC of ISIR, Osaka University, for nitrogen analysis. This research was partially supported by a Grant-in-Aid for General Science Research from the Ministry of Education, Science and Culture of Japan, by grants from the Matsuda Foundation, Iketani Science and Technology Foundation, and Tokuyama Science and Technology Foundation, and by a grant from the research project on "Nanoscale Design of Inorganic Materials" of ISIR, Osaka University.

REFERENCES

1. M. Y. Chern and F. J. Disalvo, *J. Solid State Chem.* **88,** 459 (1990).
2. S. Massidda, W. E. Pikett, and M. Posternak, *Phys. Rev. B* **44,** 1258 (1991).
3. M. Y. Chern, D. A. Vennos, and F. J. Disalo, *J. Solid State Chem.* **96,** 415 (1992).
4. A. Gudat, S. Haag, R. Kniep, and A. Rabenau, *J. Less-Common Met.* **159,** L29 (1990).
5. T. Yamamoto, S. Kikkawa, and F. Kanamaru, *Solid State Ionics* **63–65,** 148 (1993).
6. Y. Laurent, J. Lang, and M. T. Le Bihan, *Acta Crystallogr. Sect. B* **24,** 494 (1968).
7. N. E. Brese and M. O'Keeffe, *J. Solid State Chem.* **87,** 134 (1990).
8. P. W. Selwood, "Magnetochemistry," p. 186. Wiley–Interscience, New York, 1979.
9. G. J. W. R. Dorman and M. Sikkens, *Thin Solid Films* **105,** 251 (1983).
10. L. Pauling, "The Chemical Bond," pp. 136 and 150. Cornell Univ. Press, Ithaca, NY, 1967.
11. R. D. Shannon, *Acta Crystallogr. Sect. A* **32,** 751 (1976).